Influence of laser-generated surface micro-structuring on the intrinsically bonded hybrid system CFRP-EN AW 6082-T6 on its corrosion properties

Alexander Delp[*1a], Jonathan Freund[2b], Shuang Wu[3c], Ronja Scholz[4a], Miriam Löbbecke[5b], Jan Haubrich[6b] Thomas Tröster[7c], Frank Walther[8a]

[a]*TU Dortmund University, Department of Materials Test Engineering (WPT), Baroperstr. 303, 44227 Dortmund, Germany*
[b]*German Aerospace Center (DLR), Institute of Materials Research, Res. Group Materials Design and Engineering, Linder Hoehe, 51147 Cologne, Germany*
[c]*Paderborn University, Institute for lightweight design with hybrid systems, Automotive Lightweight Design (LiA), Mersinweg 7, 33100 Paderborn, Germany*

Abstract

The corrosion behavior of a hybrid material consisting of intrinsically bonded carbon fiber-reinforced epoxy resin with laser-structured EN AW 6082 metal was investigated. Particular attention was paid to the effects of the laser-structuring, surface topography and the contacting. Pristine and hybridized specimens were corroded in aqueous NaCl electrolyte (0.1mol/l) using a potentiodynamic polarization technique and subsequently analyzed using computed tomography, scanning electron-, light- and laser scanning microscopy. The results show that the corrosive reaction arises mainly from the aluminum component. Surface pretreatment of the aluminum resulted in increasing corrosion rates, but showed no influence on the hybrids corrosion properties. Optical micrographs suggest that the epoxy resin acts as a sealant preventing galvanic corrosion between the aluminum and carbon fibers by hindering the diffusion of the electrolyte into the joints. While corrosion effects were observed locally at the aluminum surface, they were, contrary to expectations, not enhanced on the hybrid interfaces.

Keywords: potentiodynamic polarization; aluminum; CFRP; materials testing; hybrid structures; corrosion; composites

1. Introduction

In order to deal with the ongoing challenge of reducing the emission of greenhouse gases like carbon dioxide or nitrogen oxides in transportation, new solutions, especially for the automotive industry need to be developed. One of the most important, recent changes was the focus on the development of efficient, electric cars, since they are not producing any emissions by themselves while being used. Nevertheless, recent studies show, that the current grid mix composition of industrialized countries still relies highly on fossil fuels, resulting in higher life cycle carbon emissions for electric- compared to fuel powered vehicles [1]. Therefore, other short-term solutions for reduction of emissions, like the development of efficient lightweight structures are necessary. Carbon fiber-reinforced polymers (CFRP) are being used in the automotive industry due to their lightweight potential and high performance, although high material costs and complex manufacturing processes still limited a widespread introduction. In combination with other lightweight materials, for example impact-resistant metals, a promising approach for cost-efficient and high-performative hybrid lightweight structures emerges [2–4]. Aluminum alloy (Al) EN-AW 6082 is a commonly used lightweight alloy in the automotive industry. It is corrosion-resistant and exhibits high mechanical strength after heat treatment, which renders it suitable for use in hybrid materials and structures in automotive applications [5,6]. However, the joint between the CFRP and the metal remains an unresolved challenge. Currently, different manufacturing techniques are employed, for example blind riveting [7], bolting, welding [8] and adhesive bonding [9]. One benefit of adhesive bonding lies in avoiding local damage (e.g., rivet holes, cracks) and weakening thermal influences (over-ageing during welding) on the material. A promising technique for cleaning, structuring and functionalization of metallic surfaces before bonding is the laser pretreatment [10]. By laser structuring the metallic surfaces, the mechanical strength of adhesive aluminum- and aluminum composite hybrid joints can be increased significantly [11,12], resulting in a broader range of possible applications for aluminum CFRP hybrid materials. Besides enhancing chemical and mechanical bonding by surface structuring and surface area enhancement, the laser pretreatment also affects the corrosion properties of the interface.

Manufacturing time and cost efficiency can be improved by exploiting optimized prepreg pressing processes with shortened curing cycles for the prepreg and enhancement of the quality of the near-net-shaped semi-finished product. Additionally, a high level of automation of the sheet metal forming process is possible [13].

[*]Corresponding author
email: alexander.delp@tu-dortmund.de; Alexander Delp
[1] ORCID: 0000-0002-2057-7806; A.D.
[2] ORCID: 0000-0002-7073-1365; J.F.
[3] ORCID: 0000-0001-8645-9952; S.W.
[4] ORCID: 0000-0001-9872-977X; R.S.
[5] ORCID: 0000-0001-7838-6204; M.L.
[6] ORCID: 0000-0002-5748-2755; J.H.
[7] ORCID: 0000-0003-3488-5575; T.T.
[8] ORCID: 0000-0003-2287-2099; F.W.

A challenge is the corrosive behavior of the multi-material composites in conjunction with aluminum: If carbon fibers (CF) are conductively connected to metal f.e. aluminum and an electrolyte is present, a galvanic element develops in which aluminum acts as anode [14]. Nonetheless, in other configurations, galvanic corrosion is possible at carbon fibers, too [15]. Blind riveted Al/CFRP structures are for instance known to be vulnerable to corrosion inside the rivet crevice [7].

In the current study we investigated the corrosion behavior of adhesively bonded aluminum CFRP hybrids, a possible influence of a laser pretreatment of the metal surface, and whether the direct bonding of epoxy-based CFRP with structured aluminum alloys allows eliminating gaps in the joint and thereby reduces the cross-section susceptible to electrolyte intrusion. The potentiodynamic polarization method (PDP), a common technique for fast characterization of corrosive properties of materials [16–18], is used to study the corrosion reaction.

2. Materials and Methods

The hybrid material was produced from laser structured EN-AW 6082-T6 sheets that were intrinsically bonded to CFRP with an epoxy matrix by a laboratory pressThe hybrid specimen were prepared for potentiodynamic polarization and subsequently characterized by various optical and tactile techniques.

2.1. Specimen manufacturing

EN-AW 6082-T6 and unidirectional, epoxy-based CFRP prepreg Sigrapreg C (U230-0/NF-E20/39%; SGL Carbon SE, Wiesbaden, Germany) were used as constituents of the hybrid joint. The manufacturing process consisted of two steps: (1) a laser structuring with previously determined parameters; (2) hybridization by pressing and curing at a defined temperature. The hybrid material was water jet cut into separated specimen for characterization.

2.1.1. Laser surface pretreatment

For the surface pre-treatment of the aluminum, a pulsed Nd:YAG-Laser CL20 (Clean Lasersysteme GmbH, Herzogenrath, Germany) with a wavelength of 1064 nm was used. During scanning the laser beam moves in meandering patterns. Therefore, scans the surface in two directions (0°, 180°).

In this study, the influence of two pre-selected laser pre-treatments with different laser parameters derived in a separate study were employed that lead to qualitatively different surface structures. A laser power P, an overlap o of the laser spots and a number of scans N were used as follows: parameter set 1 (P1): P = 20W, o = 10%, N = 5; Parameter set 2 (P2): P = 15W, o = 50%, N = 1. The frequency of the pulsed laser was set to f = 60 kHz. The resulting cross section of the pre-treated aluminum are analyzed in chapter 3.3 and are referred to as “ordered” (P1) and “disordered structure” (P2).

2.1.2. Hybridization

For hybridization (joining), the prepreg pressing process described in ref. [13] was used. Therefore, the prepreg (stored in a refrigerator) was cut and placed in six layers (thickness d = 0.23 mm, each) on 2 mm thick, laser-structured aluminum sheets. The included EP is used as an adhesive. The multi-layer composite was placed subsequently inside a three-plate mold with a mold cavity of 70.2 × 70.2 mm^2, see Fig. 1. The mold was preheated to the process temperature of ϑ = 150 °C in a laboratory press (LaboPress P200s, VOGT Labormaschinen GmbH, Berlin, Germany). After that, the mold tool was placed with the composite inside the laboratory press. The following manufacturing parameters were chosen: time t = 5 min, temperature ϑ = 150°C, and pressure p = 0.3 MPa. To simulate the real manufacturing process in a series production as far as possible, the post-curing parameters were determined based on the electrophoretic dip-painting process in the automotive industry, namely temperature: ϑ = 180°C and time t = 30 min.

(Please place fig. 1 here, width: 1/2 page/1 column/8cm)

2.1.3. Specimen preparation

To describe the effect of hybridization on the corrosion behavior, a comparison between different surfaces, conductivity and heat treatments of the monolithic materials EN-AW 6082 and CFRP is necessary. In order to provide basic data, different properties were tested: First, the conductivity of EN-AW 6082-T6 was increased by soldering a braid onto the back, of an untreated surface. No fluxing agent was used, to minimize unknown influences. Air contact and thereby an oxidation was prevented using cutting oil on the surface. The existing oxide layer was reduced using sand paper with a grit size (ISO) of 240. After heating the material up to ~400 °C, the braid was attached with solder. For comparison with other results from PDP (polished specimen), structured and non-structured surfaces and to prevent residual stresses from the grinding process, EN AW 6082 specimens were electrolytically polished (ep) (LectroPol-5, Struers GmbH, Willich, Germany), using electrolyte A2 (Struers GmbH, Willich, Germany), containing perchlorid acid, ethanol and water. Polishing parameters were chosen as follows: flow rate: 16 l/min, voltage: 27 V, Area: 2 cm^2, temperature: − 15°C, time: 15s.

As a CFRP layer is not suitable for electrochemical polishing and the relevant area is the interface of the hybrid material, the specimens were cleaned with ethanol, embedded in epoxy resin and grinded with sand paper (grid size (ISO) 320, 800, 1200, 2500) before polishing manually (mp) (particle size 6 µm, 3 µm, 1 µm).

2.2. Roughness measurement

The surface roughness was determined using a mobile Marsurf M300C device with software version V.3.12-04 and stylus PTH 6-350/2µm (all Mahr GmbH, Göttingen, Germany), primarily to qualify different surface characteristics regarding waviness and roughness. Each surface type was tested in two directions, three times each, with a stylus travel l_t = 5.6 mm and a cutoff of 0.8 mm, based on ISO 4288. Between every scan the hand device was manually elevated and rearranged. For Al, rolled (untreated) and electrolytically polished surfaces, for CFRP untreated and for polished hybrid material three specimens with two types of laser structuring (CFRP and aluminum independently) were analyzed. Analyses of non-bonded materials were carried out for two directions. The 0° direction has been chosen as following: aluminum, (non-structured and polished): rolling direction; CFRP: fiber direction; laser-structured surface: longitudinal direction of specimen. The mean roughness was averaged over three measurements for each orientation and surface.

2.3. Corrosion Testing

For PDP, a Gamry G300 and Interface 1000 potentiostat (Gamry Instruments Inc., Warminster, PA, USA) was used in a three-electrode setup with an Ag/AgCl reference (RE-1CP, ALS Co., Ltd, Tokyo, Japan). The specimens were installed as working electrode. A glassy-graphite pin electrode served as counter electrode. For validation, the constancy of the potential of the reference electrode measured against a saturated Calomel electrode (SCE; +0.242 V vs. Standard hydrogen electrode (SHE) [19]; RE-2BP, ALS Co., Ltd, Tokyo, Japan) was confirmed as 47.5 mV. The electrochemical setup was arranged inside of a customized acrylic glass corrosion cell developed by the authors of [20] (Fig. 2). With an electrolyte volume of 600 ml. The specimens were attached via a brazed threaded rod to ensure good conductivity and pressed against a round notch sealed with an O-ring. The reference electrode was placed inside a Luggin capillary with an opening fixed close to the specimen surface. An aqueous solution of 0.1mol/l NaCl in deionized H_2O served as electrolyte. The specimens were cleaned previously in ethanol (purity 99,9%). According to ISO 17475, a time of one hour was used to stabilize the open circuit potential (OCP) before starting the PDP measurement with a potential feed $\Delta\dot{E}$ = 1 mVs^{-1} and a potential range ΔE of ± 300 mV (measured against OCP). Due to passivation effects, the slope of the anodic part of Tafel plot was fitted and used to determine the corrosion current density i_{corr} at the intersection with OCP.

(Please place fig. 2 here, width: 1/2 page/1 column/8cm)

2.4. Topography analysis methods

Three different imaging methods and computed tomography were used to characterize the prepared surfaces, the joint interfaces as well as the results of the corrosion reaction of the material. The topography of the surface was characterized by laser scanning microscopy (LSM) and scanning electron microscopy (SEM). To avoid sputter coating, also light microscopy (LM) was used in order to prevent specimen destruction due to sputter coating and characterize the CFRP as well as the interface area.

2.4.1. Laser scanning microscopy

In order to characterize the topography of the laser generated surface structures, a confocal laser scanning microscope (LSM) 700 (Carl Zeiss Microscopy GmbH, Oberkochen, Germany) was used. For the analysis of the aluminums surface, a laser wavelength of 405 nm, a laser power of 0.5 mW and a pinhole of 7.5 mm was chosen. The LSM enables to create “z-stacks”, which are 3D scans of the surface, stitched together from single images taken in intervals of 0.1 µm to 0.25 µm between the lowest and the highest point of the surface structure. An area of 319×319 µm² was scanned per z-stack.

The raw data produced by LSM still shows so called “spikes”, which are error peaks indicating a false height profile. Therefore, it was further post-processed with the respective software ConfoMap (Carl Zeiss Microscopy GmbH, Oberkochen, Germany). A gaussian low pass filter (0.8 µm) was applied to filter out high frequency contributions. The 2D-roughness parameters (R_z, R_a) were subsequently calculated according to ISO 25178-2:2012.

2.4.2. Scanning electron microscopy

For this study, SEM Mira 3 XMU (Tescan, Dortmund, Germany) that provides high imaging quality. In order to increase conductivity, the specimens were carbon coated (Cressington Carbon Coater CR208 carbon, Tescan, Dortmund, Germany).

2.4.3. Light microscopy

In order to retain color information, corroded and non-corroded areas were measured using digital LM VHX-500X with VH-Z20R and VH Z500R lenses (Keyence, Osaka, Japan).

2.4.4. Computed tomography

For non-destructive 3D micro computed tomography (CT) analysis, a Nikon XTH-160 was used with corresponding software Inspect X (version XT 4.4.4) for imaging and CT-Pro 3D (version XT 4.4.4) for reconstruction (Nikon Metrology Europe NV, Leuven, Belgium). Visualization and post-processing were conducted using VG Studio MAX, version 2.2.4 (Volume Graphics GmbH, Heidelberg, Germany). The following CT scanning parameters were chosen:
Resolution: 1008 px × 1008 px; 15 µm/px, voltage: 105 kV, current: 95 µA, exposure: 500 ms, 360° Scan with 1583 projections, 8 frames/projection.

CT thus enables a non-destructive investigation of the interface between CFRP and aluminum as shown in Fig. 3, to reconstruct a 3D image of the specimen with a resulting voxel size of 15 × 15 × 15 μm^3 (Fig. 3 b) and digitally hide a layer (Fig. 3 c). The hybridized specimen consists of three important regions: the CFRP volume, the aluminums volume and the interface between the materials.

(Please place fig. 3 here, width: 1 page/ 16cm)

3. Results

For further classification of OCP and i_{corr} results gained by potentiodynamic polarization, the surface condition of the specimens was compared pre and post corroding as well as pre and post hybridization. PDP provided electrical values and by use of optical methods it was further possible, to locate corrosion products, characterize surface conditions and adhesive bonding.

3.1. Two-Dimensional-characterization of aluminum surface

Depending on the surface conditions LM and SEM show different appearances. Those are depicted in Fig. 4. The pristine surface of the rolled aluminum is characterized by grooves and a metallic shine (Fig. 4 a). Moreover, pits can be seen distributed over the whole surface. The color observed in LM is different between untreated, grooved and pitted areas (Fig. 4 b). While SEM allows a much higher resolution, the missing color information from optical imaging prevents finding the pits quickly (Fig. 4 c). In SEM the laser-structured surface (Fig. 4 d) presents its characteristic structure of ridges and valleys (Fig. 4 e) known for instance also from laser pretreated titanium surfaces [21]. The high roughness and functionalization, i.e., the oxide surface layers formed by laser treatment on air, leads to a dull grey shine of the treated area on the specimens.

The reduction of the surface roughness by electropolishing, in contrast, leads to a shiny metallic surface. Etching pits are formed due to local dissolution of material in the vicinity of silicium particles (Fig. 4 f) [22,23].

(Please place fig. 4 here, width: 1/2 page/1 column/8cm)

3.2. Surface roughness

The one-dimensional surface roughness, here represented by the maximum height amplitude R_z, differs depending on the surface treatment, as visible in Fig. 5. The roughness of the pure, untreated CFRP, the rolled and the electro-polished aluminum sheet are comparable. The roughness is slightly higher perpendicular to manufacturing direction (90°) for the mentioned surfaces.

The laser-structured surfaces are much rougher. The mean roughnesses R_z are distinctly higher for both sets of laser parameters P1 and P2 than for the other treatments and show a strong anisotropy regarding the surface orientation. Furthermore, although the prior mechanical preparation (mp) of the surface was the same, aluminum and CFRP show different R_z in initial condition. The surfaces of CFRP and rolled EN-AW 6082 shows randomly distributed highs and lows with moderate manifestation, but strongly oscillates for laser-structured aluminum, shown with Fig. 6. For the laser pretreated condition P1 of the EN-AW 6082 specimens, a higher oscillation of the measured height amplitudes is observed than for P2.

(Please place fig. 5 here, width: 1/2 page/1 column/8cm)

(Please place fig. 6 here, width: 1 page/16cm)

Three-dimensional characterization of aluminum surfaces

The two structures generated by laser pre-treatment with the laser parameter sets P1 and P2 lead to different surface structures that can be described as ordered, periodic for P1 and appear very disordered for P2, see Fig. 7). While the ordered structure presents a high periodicity in x- and y-direction and visible craters, the disordered structure has almost no visible recurring structure motives. While the scanning direction of the laser used for the surface pre-treatment is clearly visible in the ordered structure, it can only barely be discerned on the surfaces treated with laser parameter P2. On the P1 treated specimens, the meandering laser paths lead to a surface pattern consisting of high, almost linear structures, which are parallel to the scanning direction.

Another key difference between the two structures is the maximum height S_z of the surface topographies. The ordered structure has a maximum height of S_z = 59.9 µm. The disordered structure has a maximum height of S_z = 16.2 µm, and is, thus, much smoother. When comparing the arithmetic mean height of the structures, the disordered structure reaches approximatelys one fifth of the ordered structure's mean height, given the values of $S_{a,ordered}$ = 7.5 µm and $S_{a,disordered}$ = 1.3 µm.

(Please place fig. 7 here, width: 1 page/16cm, please use color)

(Please place fig. 8 here, width: 1 page/16cm)

3.3. Inner volume condition

With CT it is possible to distinguish between the laser pretreated structures by segmenting the data by specific material regions and selected representation of single layers as seen in Fig. 8. CT reveals that the surface structures remains untouched within the achieved resolution after hybridization. No visible voids were detected at the interface. The nanostructures formed by the laser pretreatement cannot be assessed by µ-CT. The carbon fibers are not evenly distributed within the whole CFRP layer and regions are found that deplete of fibers but instead only filled with polymer matrix from the epoxy precursor, as shown in Fig. 9. Importantly, also the interface region between the dissimilar materials appears well infiltrated by the matrix that is readily identifyable in Fig. 10 as dark background. The different laser surface structures are also distinguishable: while the initial surface is smooth (Fig.10 a), P1 results in evenly distanced grooves (Fig.10 b) and P2 produces a merely a aperiodic, rough surface (Fig. 10 c).
Notably, the results show that the polymer matrix has formed a separating layer ~10 µm without any fibers that in addition to the surface functionalization can act as insulating layer between the CF and the metal substrate. Nonetheless, the fiber distribution follows the surface structure.

(Please place fig. 9 here, width: 1/2 page/1 column/8cm)
(Please place fig. 10 here, width: 1/2 page/1 column/8cm)

3.4. Corrosion

For the corrosion investigations, different surface states and contacting conditions were considered. The results of PDP measurements are shown using Tafel-plots on a semi-logarithmic scale in Fig. 11. Since polishing the specimens would lead to destruction of the relevant surface structures, it is not possible to polish them and, therefore conduct PDP measurement with polished specimens. Thus, EN-AW 6082T6 was used in initial condition for reference, i.e., only after removing the protective plastic film and cleaning the surface with ethanol.

The mean values and standard deviations of OCP's and i_{corr} for varying surface and contacting conditions of EN AW 6082 are listed in tab. 1.

(Please table 1 here)

Contacting improves the conductivity and, thereby, seems to reduce the corrosion, as the current density as well as the OCP decreases. Equally, a polished surface results in a decrease of electrochemical parameters and STD. No reliable influence of heating could be detected.

The OCP's and i_{corr} mean values for CFRP, non-structured, and structured surfaces (P1, P2), as well as the corresponding hybrid composites are listed in tab. 2. The resulting Tafel-plots are shown with Fig. 12. Further Tafel-plots regarding the hybrid-composites can be found in Appendix A, Fig. 14.

(Please place table 2 here)

Comparing the hybrid specimen surfaces pre- and post-corroding, depicted with Fig. 13 the resulting damage from the corrosion processes are identified. They are observed in form of small pits that spread out over the whole surface. There is no enhanced corrosion visible in the interface region of the hybrid joints.

(Please place fig. 11 here, width: 1 page/16cm)
(Please place fig. 12 here, width: 1 page/16cm)
(Please place fig. 13 here, width: 1 page/16cm)

4. Discussion

The position of CFRP in the Tafel plot differs strongly from the position of hybrid and monolithic aluminum material consistent with previous studies [7,16]. Additionally, with increasing surface quality (decreasing roughness), OCP as well decreases. At the surface of the hybrid specimen i_{corr} is higher compared to that of monolithic materials. Here i_{corr} is used in a qualitative way to characterize differences in corrosion properties. OCP also decreases compared to pristine aluminum surface and reaches the same values as recorded for ep specimen. This suggest, that the polishing of surface of hybrid specimens led to the drop in OCP. According to the findings regarding the surface roughness, also the OCP for structured surfaces (P1, P2) increases. The electrochemical values of the hybrid material are close to the values of the EN-AW 6082 component. Therefore, it is concluded that the corrosion process originates mainly from the aluminum component. [16,24]

Results from LM regarding the corrosion products underline these findings. Heating of the Al component seems to have no reproducible influence on the OCP, but i_{corr}. Therefore, the observed differences in OCP for specimens with soldered contact can be traced back solely to the contacting. The decrease of i_{corr} corresponding to decreasing surface roughness detected in PDP measurements can be explained by observing the determination of i_{corr}, using the contact area as a calculation factor. The measured 2D area of a structured specimen is not equal to the real surface area due to the 3D nature of non-polished specimens, which is not considered within the application-oriented measuring of corrosion areas via 2D microscopy. The determination of the true surface area is part of an ongoing study.

The 3D LSM profiles complement the one-dimensional roughness profiles (R_z) with information in the lateral directions (S_z). It can be seen, that i_{corr} correlates with the increase of R_z and S_z on the metal surface. While the laser parameter set P1 (highest S_z)

results in a higher i_{corr} and, therefore, tendentially in a higher mass lost, the OCP is decreased in comparison to the less rough, disordered surface, generated with laser parameter set P2. This higher OCP indicates, that both of the laser-generated surface structures lead to a less noble characteristic. The drop in i_{corr} in comparison with non structured material and structure P2, but not for P1, despite both structures lead to an enhanced surface area, indicate, that P2 could lead to an improvement of the hydrophobicity of the aluminum as it is the case for some specially designed laser- or chemically generated structures [25,26]. To confirm this assumption, more investigations are necessary. The OCP of ep and hybrid specimen is within the same value range. The same applies to the comparison between pristine, P1 and P2 structured hybrid specimen. The Tafel plots and, consequently the corrosion values (OCP, i_{corr}) are located within the same range. Therefore, it can be concluded, that different surface structuring on the macroscopic scale has no influence on the corrosive properties between different hybrid specimens.

i_{corr} is used for the qualitative assessment of microstructural differences between different surface and contacting conditions. The OCP seems unaffected by the random distribution of surface structures, but not by the surface overall condition (f.e. polished, P1, P2).

In contrary to the blank metal surface, the OCP and i_{corr} of the hybrid material shows no significant difference between the differently pretreated aluminum sheets. Both of the laser structured, as well as the non-structured specimen show an OCP value of approximately −600 mV and a mean corrosion current density i_{corr} around 5×10^{-6} Acm^{-2}. This indicates that the CFRP matrix, bonded to the aluminum surface acts as a corrosion inhibitor regarding direct contact between fiber and metal surface. Several studies on different aluminum alloys and steel report a similar effect and furthermore worked on possible enhancements. [27–29]. The higher values for i_{corr} of hybrid specimens, compared to structured Al surfaces and CFRP support the assumption, that, despite the insulating layer, direct contacts between CFRP and blank metal is possible [30]. Validating µCT data using light microscopy, it was possible to show, that the CFRP is bonded at the Al surface without detectable voids.

5. Conclusion and outlook

This study provides first insights on the corrosion behavior of intrinsically bonded CFRP/EN-AW-6082 hybrid structures from PDP measurements. The corrosion behavior is affected by the surface structuring, despite aluminum is predominantly sealed by the plastic component against direct contact with CF. The corrosion occurs locally, but is distributed over the whole surface (pitting corrosion). To separate the contributing mechanisms, different surface conditions were tested. For the PDP methodology, optimized contacts and polished, smooth surfaces are suggested in order to minimize background noise and obtain more precise measurements. However, these suggestions cannot be implemented when investigating structured surfaces in the structured layer.

For the laser-structured hybrid specimen it can be concluded that the surface structuring seems to have no influence on the short time (PDP) corrosion properties. Therefore, future hybrid aluminum-CFRP materials can be produced with a laser-pretreatment benefiting from its positive influence on the mechanical strength without affecting the corrosion. If the corrosion will be a problem for the long-term stability of the interface in the hybrid material, further investigations on the design of hydrophilic, laser-generated structures should be conducted.

Furthermore investigations regarding the adhesive strength of different laser structures, as well as the influence of hybridization parameters are necessary to evaluate and rate the overall parameters for an optimal process window for laser structuring and hybridization under consideration of environmental influences. Additionally, it is of prime importance to determine the true accessible surfaces of structured surfaces.

Author Contributions

Conceptualization: R.S., M.L, J.H., T.T., F.W., Methodology: A.D., J.F., S.W., Investigation: A.D., J.F., Writing - Original Draft: A.D., J.F., S.W, Writing - Review & Editing: R.S., M.L., J.H., T.T., F.W., Visualization: A.D., Supervision: J.H., T.T., F.W., Funding acquisition: J.H., T.T., F.W. All authors have read and agreed to the published version of the manuscript.

Funding

The research project is funded by the Deutsche Forschungsgemeinschaft (DFG, German Research Foundation) – Project number - 426499947 - “Energy-efficient manufacturing and mechanism-based corrosion fatigue characterization of laser-structured hybrid structures“ (HA 5600/5-1, TR 373/9-1, WA 1672/65-1).

Acknowledgements

Conflict of interests

The Authors declare no conflict of interests

Data availability

The raw/processed data required to reproduce these findings cannot be shared at this time as the data also forms part of an ongoing study.

Appendix A

(Please place fig. 14 here, width: 1 page/16cm)

6. References

[1] Li Y, Ha N, Li T. Research on Carbon Emissions of Electric Vehicles throughout the Life Cycle Assessment Taking into Vehicle Weight and Grid Mix Composition. Energies 2019;12(19):3612. https://doi.org/10.3390/en12193612.

[2] Vermeeren CAJR. Applied Composite Materials 2003;10(4/5):189–205. https://doi.org/10.1023/A:1025533701806.

[3] Mrzljak S, Schmidt S, Kohl A, Hülsbusch D, Hausmann J, Walther F. Testing Procedure for Fatigue Characterization of Steel-CFRP Hybrid Laminate Considering Material Dependent Self-Heating. Materials (Basel) 2021;14(12). https://doi.org/10.3390/ma14123394.

[4] Min J, Li Y, Li J, Carlson BE, Lin J. Friction stir blind riveting of carbon fiber-reinforced polymer composite and aluminum alloy sheets. Int J Adv Manuf Technol 2015;76(5-8):1403–10. https://doi.org/10.1007/s00170-014-6364-8.

[5] Xhanari K, Finšgar M. The Corrosion Inhibition of AA6082 Aluminium Alloy by Certain Azoles in Chloride Solution: Electrochemistry and Surface Analysis. Coatings 2019;9(6):380. https://doi.org/10.3390/coatings9060380.

[6] Fundamentals of Aluminium Metallurgy. Elsevier; 2018.

[7] Li S, Khan HA, Hihara LH, Cong H, Li J. Corrosion behavior of friction stir blind riveted Al/CFRP and Mg/CFRP joints exposed to a marine environment. Corrosion Science 2018;132:300–9. https://doi.org/10.1016/j.corsci.2018.01.005.

[8] Pramanik A, Basak AK, Dong Y, Sarker PK, Uddin MS, Littlefair G et al. Joining of carbon fibre reinforced polymer (CFRP) composites and aluminium alloys – A review. Composites Part A: Applied Science and Manufacturing 2017;101:1–29. https://doi.org/10.1016/j.compositesa.2017.06.007.

[9] Park SY, Choi WJ, Choi HS, Kwon H, Kim SH. Recent Trends in Surface Treatment Technologies for Airframe Adhesive Bonding Processing: A Review (1995–2008). The Journal of Adhesion 2010;86(2):192–221. https://doi.org/10.1080/00218460903418345.

[10] Rechner R, Jansen I, Beyer E. Influence on the strength and aging resistance of aluminium joints by laser pre-treatment and surface modification. International Journal of Adhesion and Adhesives 2010;30(7):595–601. https://doi.org/10.1016/j.ijadhadh.2010.05.009.

[11] Heckert A, Zaeh MF. Laser Surface Pre-treatment of Aluminium for Hybrid Joints with Glass Fibre Reinforced Thermoplastics. Physics Procedia 2014;56:1171–81. https://doi.org/10.1016/j.phpro.2014.08.032.

[12] Steinert P, Dittes A, Schimmelpfennig R, Scharf I, Lampke T, Schubert A. Design of high strength polymer metal interfaces by laser microstructured surfaces. IOP Conf. Ser.: Mater. Sci. Eng. 2018;373:12015. https://doi.org/10.1088/1757-899X/373/1/012015.

[13] Christian Lauter. Development and production of hybrid components of metal and fiber reinforced plastics for the lightwight construction in automotive industries (in german). Paderborn; 2014.

[14] Mandel M, Krüger L. Determination of pitting sensitivity of the aluminium alloy EN AW-6060-T6 in a carbon-fibre reinforced plastic/aluminium rivet joint by finite element simulation of the galvanic corrosion process. Corrosion Science 2013;73:172–80. https://doi.org/10.1016/j.corsci.2013.03.033.

[15] Gebhard A, Bayerl T, Schlarb AK, Friedrich K. Galvanic corrosion of polyacrylnitrile (PAN) and pitch based short carbon fibres in polyetheretherketone (PEEK) composites. Corrosion Science 2009;51(11):2524–8. https://doi.org/10.1016/j.corsci.2009.05.051.

[16] Kim Y, Yoo M, Moon M. Effects of Surface Roughness on the Electrochemical Properties and Galvanic Corrosion Behavior of CFRP and SPCC Alloy. Materials (Basel) 2020;13(18). https://doi.org/10.3390/ma13184211.

[17] Wu X, Sun J, Wang J, Jiang Y, Li J. Investigation on galvanic corrosion behaviors of CFRPs and aluminum alloys systems for automotive applications. Materials and Corrosion 2019;70(6):1036–43. https://doi.org/10.1002/maco.201810635.

[18] Narsimhachary D, Rai PK, Shariff SM, Padmanabham G, Mondal K, Basu A. Corrosion Behavior of Laser-Brazed Surface Made by Joining of AA6082 and Galvanized Steel. J. of Materi Eng and Perform 2019;28(4):2115–27. https://doi.org/10.1007/s11665-019-03962-y.

[19] McCafferty E. Introduction to Corrosion Science. New York, NY: Springer New York; 2010.

[20] Wegner N, Kotzem D, Walther F. Corrosion and corrosion fatigue properties of the additively manufactured magnesium alloy WE43 for biomedical applications (in german). In: Werkstoffprüfung 2019 - Fortschritte in der Werkstoffprüfung für For-schung und Praxis, p. 161–166.

[21] Haubrich J, Löbbecke M, Watermeyer P, Wilde F, Requena G, Da Silva J. Buried interfaces – A systematic study to characterize an adhesive interface at multiple scales. Applied Surface Science 2018;433:546–55. https://doi.org/10.1016/j.apsusc.2017.10.015.

[22] Zhu H, Zhang X, Couper MJ, Dahle AK. Effect of Initial Microstructure on Surface Appearance of Anodized Aluminum Extrusions. Metall and Mat Trans A 2009;40(13):3264–75. https://doi.org/10.1007/s11661-009-9976-0.

[23] Österreicher JA, Kumar M, Schiffl A, Schwarz S, Hillebrand D, Bourret GR. Sample preparation methods for scanning electron microscopy of homogenized Al-Mg-Si billets: A comparative study. Materials Characterization 2016;122:63–9. https://doi.org/10.1016/j.matchar.2016.10.020.

[24] Mokhtari S, Karimzadeh F, Abbasi MH, Raeissi K. Development of super-hydrophobic surface on Al 6061 by anodizing and the evaluation of its corrosion behavior. Surface and Coatings Technology 2017;324:99–105. https://doi.org/10.1016/j.surfcoat.2017.05.060.
[25] Yang Z, Liu X, Tian Y. Hybrid Laser Ablation and Chemical Modification for Fast Fabrication of Bio-inspired Super-hydrophobic Surface with Excellent Self-cleaning, Stability and Corrosion Resistance. J Bionic Eng 2019;16(1):13–26. https://doi.org/10.1007/s42235-019-0002-y.
[26] Dagdag O, Hsissou R, Berisha A, Erramli H, Hamed O, Jodeh S et al. Polymeric-Based Epoxy Cured with a Polyaminoamide as an Anticorrosive Coating for Aluminum 2024-T3 Surface: Experimental Studies Supported by Computational Modeling. J Bio Tribo Corros 2019;5(3). https://doi.org/10.1007/s40735-019-0251-7.
[27] Zeng D, Liu Z, Zou L, Wu H. Corrosion Resistance of Epoxy Coatings Modified by Bis-Silane Prepolymer on Aluminum Alloy. Coatings 2021;11(7):842. https://doi.org/10.3390/coatings11070842.
[28] Zhang J, Zhang W, Wei L, Pu L, Liu J, Liu H et al. Alternating Multilayer Structural Epoxy Composite Coating for Corrosion Protection of Steel. Macromol. Mater. Eng. 2019;304(12):1900374. https://doi.org/10.1002/mame.201900374.
[29] Zhang C, Zheng D-J, Song G-L. Galvanic Effect Between Galvanized Steel and Carbon Fiber Reinforced Polymers. Acta Metall. Sin. (Engl. Lett.) 2017;30(4):342–51. https://doi.org/10.1007/s40195-017-0539-x.

Figure captions

Fig. 1: Three plate mold tool, composed of a punch a), sealing frame b) and die c).

Fig. 2: Customized corrosion cell with opening for specimen placement, consisting of a) working electrode (specimen), b) reference electrode, c) counter electrode, d) Luggin capillary, e) electrolyte.

Fig. 3: Macroscopic 2D visualization of an intrinsically bonded CFRP-Al hybrid specimen without laser surface structuring (a) and 3D CT-reconstruction (b), including digital removing of CFRP for non-destructive visualization of interface section (c).

Fig. 4: Optical analysis of different surface finishes: a) rolled, macroscopic; b) rolled, LM, c) rolled, SEM; d) laser-structured, macroscopic, SEM; e) laser-structured, SEM; f) electropolished, LM.

Fig. 5: Mean R_z values of investigated surface conditions averaged from data of three specimens each as a function of the measuring orientation.

Fig. 6: Qualitative comparison of characteristic roughness profiles in the 0° orientation (working direction of the laser).

Fig. 7: LSM images constructed from z-stacks of the ordered (P1) and disordered (P2) pretreatments of the AW6082-T6 surface.

Fig. 8: Surface condition of Al within a bonded CFRP/Al hybrid with digitally removed CFRP layer for a) non-structured and b), c) laser-structured material, b) parameter set 1, c) parameter set 2.

Fig. 9: Irregular shift of carbon fibers a) in longitudinal direction (top view) via LM and b) in fiber direction (front view) via CT.

Fig. 10: Close-up of the CFRP (left side)/Al (right side) interface with different surface structuring of Al (top) and detailed view on the fiber-Al distances (bottom), for a) a non-structured surface, b) parameter set 1 and c) parameter set 2.

Fig. 11: Condition of CFRP (top)/Al (bottom) hybrid material before and after corrosion as viewed from the specimens' top: Without structuring: a) initial, b) corroded; Parameter 1: c) initial, d) corroded; Parameter 2: e) initial, f) corroded.

Fig. 12: Tafel plot of EN AW 6082-T6 with varying surface and contacting condition: initial condition without treatment, electrolytically polished (ep), soldered and heated.

Fig. 13: Tafel plot of non-structured (Al, rolled), structured (Al, P1; Al, P2), CFRP and CFRP/Al hybrids with no structuring (hybr. init.), parameter set 1 (Al, hybr. P1) and 2 (Al, hybr. P2) vs. initial condition (init.).

Fig. 14: Tafel plot of three PDP-measurements for pristine, P1 and P2 hybrids.

Tables

Table 1: OCP and i_{corr} for varying surface and contacting condition of EN AW 6082.

condition	Mean OCP [mV]	σ OCP [mV]	mean i_{corr} [Acm^{-2}]	σ i_{corr} [Acm^{-2}]
rolled	−638	13	7.84×10^{-7}	6.97×10^{-7}
ep	−589	2	4.00×10^{-7}	1.20×10^{-7}
heated	−641	14	1.41×10^{-6}	1.14×10^{-6}
soldered	−599	12	2.24×10^{-6}	1.59×10^{-6}
ep, heated	−585	47	1.25×10^{-6}	1.34×10^{-6}
ep, soldered	−505	11	4.59×10^{-8}	5.58×10^{-8}

Table 2: OCP and i_{corr} for varying structuration and CFRP-EN AW 6082 hybrids

condition	mean OCP [mV]	σ OCP [mV]	mean i_{corr} [Acm^{-2}]	σ i_{corr} [Acm^{-2}]
hybrid, rolled	−606	9	5.81×10^{-6}	3.19×10^{-6}
Al, P1	−742	19	7.36×10^{-6}	4.50×10^{-6}
hybrid, P1	−595	8	5.17×10^{-6}	4.49×10^{-6}
Al, P2	−757	26	2.57×10^{-7}	1.59×10^{-7}
hybrid, P2	−614	10	5.36×10^{-6}	4.97×10^{-6}
CFRP	−171	6	1.12×10^{-7}	6.49×10^{-8}

Figures

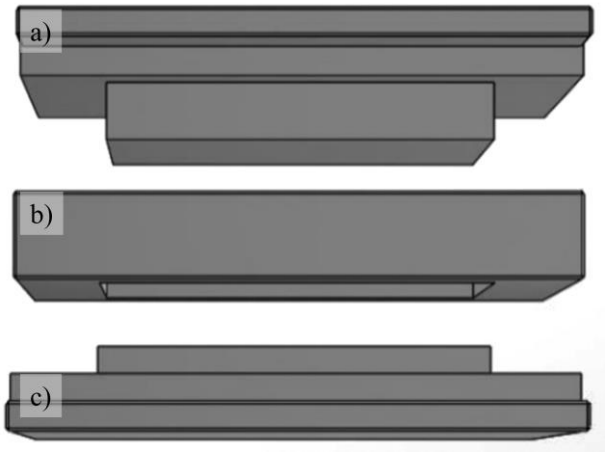

Figure 1: Three plate mold tool, composed of a punch a), sealing frame b) and die c).

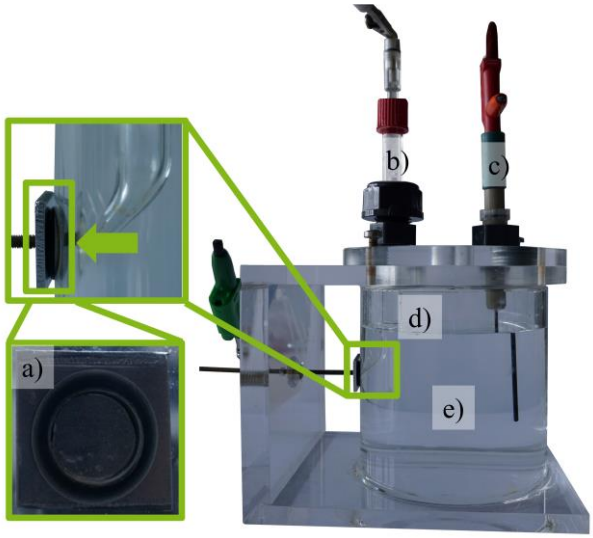

Figure 2: Customized corrosion cell with opening for specimen placement, consisting of a) working electrode (specimen), b) reference electrode, c) counter reference electrode, c) counter electrode, d) Luggin capillary, e) electrolyte.

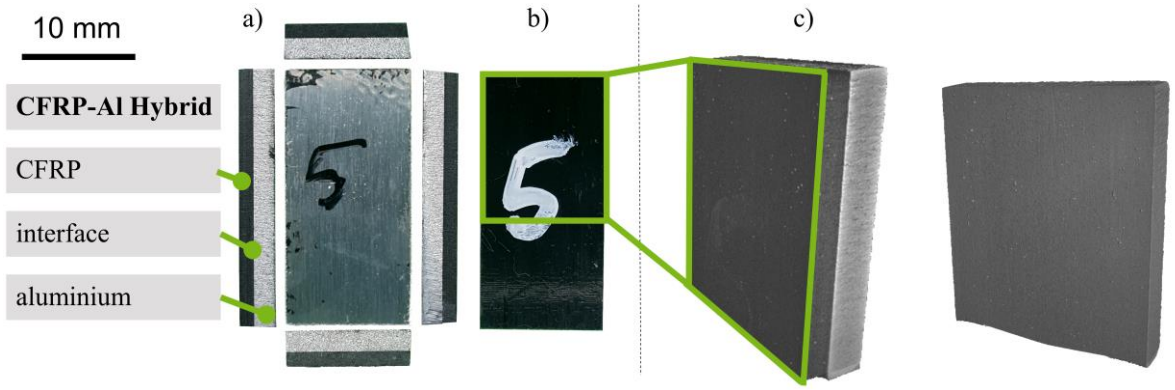

Figure 3: Macroscopic 2D visualization of an intrinsically bonded CFRP-Al hybrid specimen without laser surface structuring (a) and 3D CT-reconstruction (b), including digital removing of CFRP for non-destructive visualization of interface section (c).

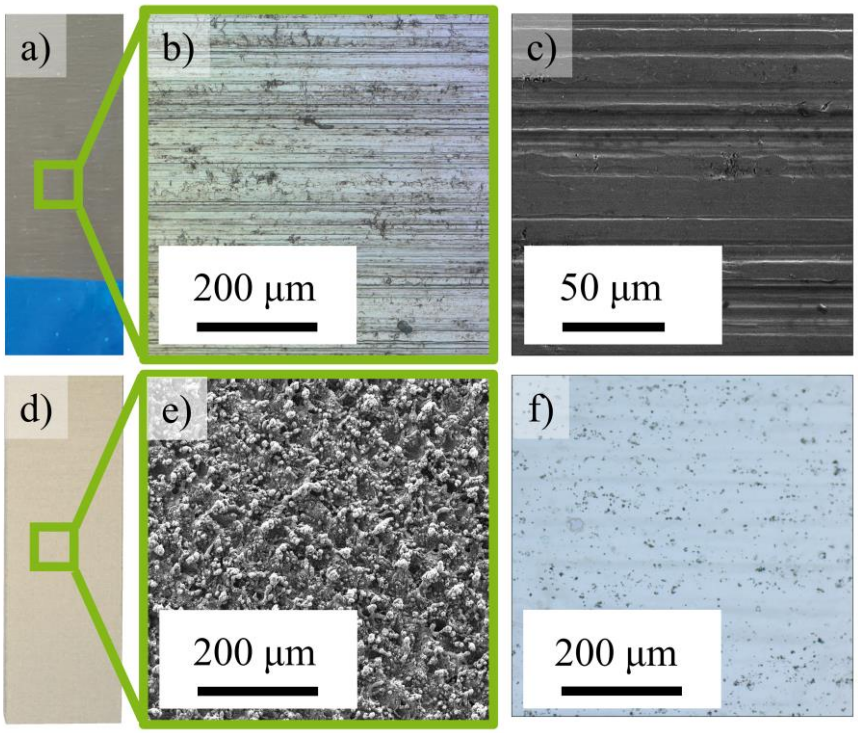

Figure 4: Optical analysis of different surface finishes: a) rolled, macroscopic; b) rolled, LM, c) rolled, SEM; d) laser-structured, macroscopic, SEM; e) laserstructured, SEM; f) electropolished, LM.

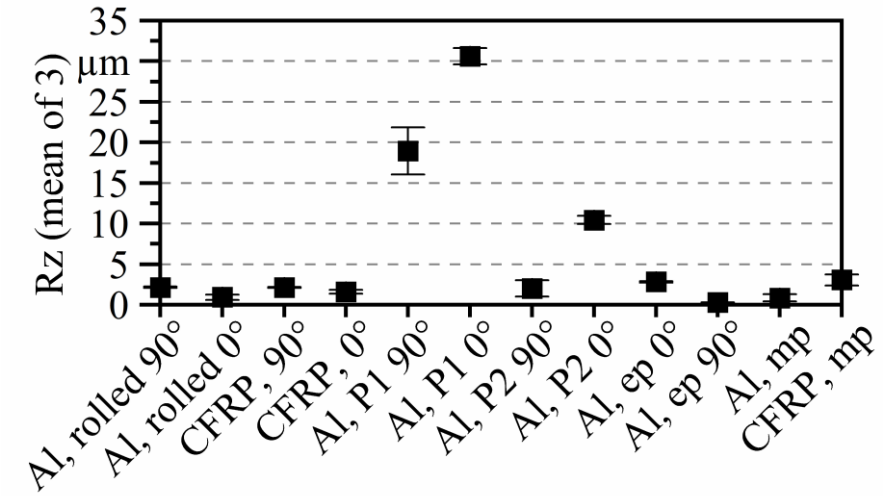

Figure 5: Mean Rz values of investigated surface conditions averaged from data of three specimens each as a function of the measuring orientation.

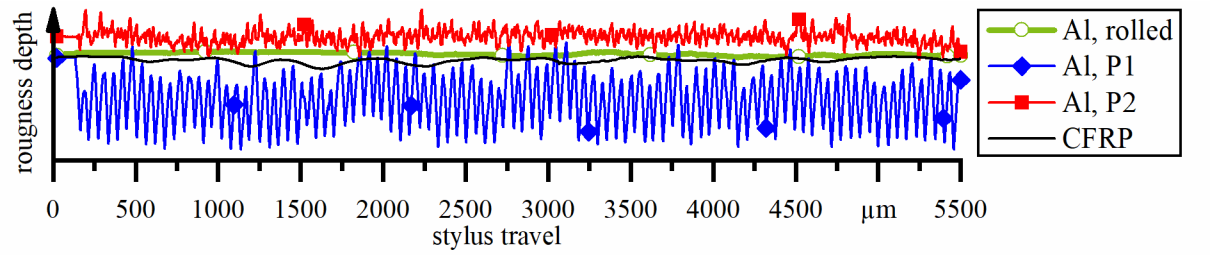

Figure 6: Qualitative comparison of characteristic roughness profiles in the 0◦ orientation (working direction of the laser).

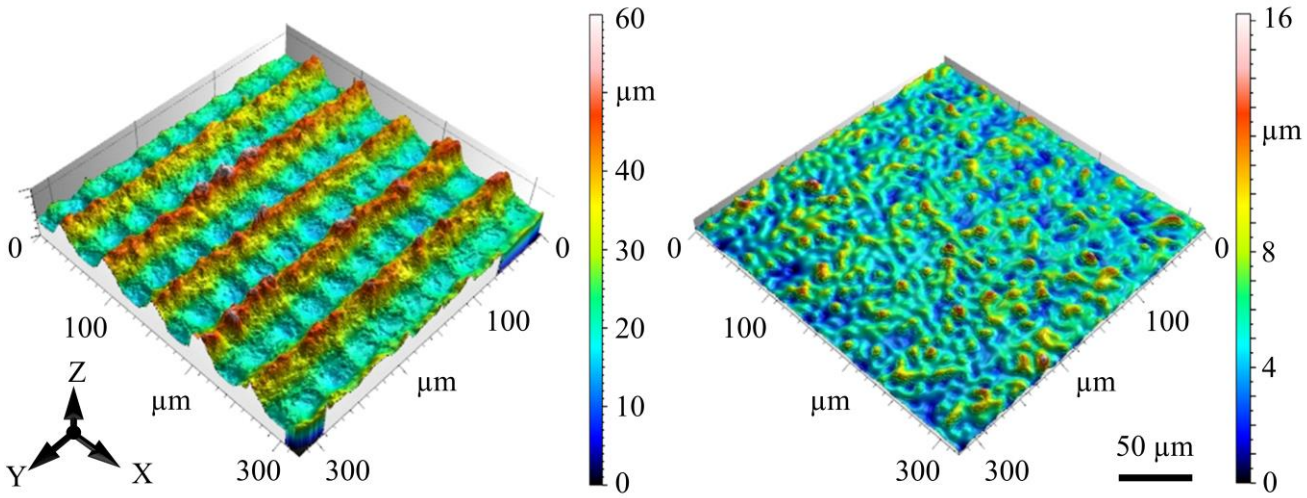

Figure 7: LSM images constructed from z-stacks of the ordered (P1) and disordered (P2) pretreatments of the AW6082-T6 surface.

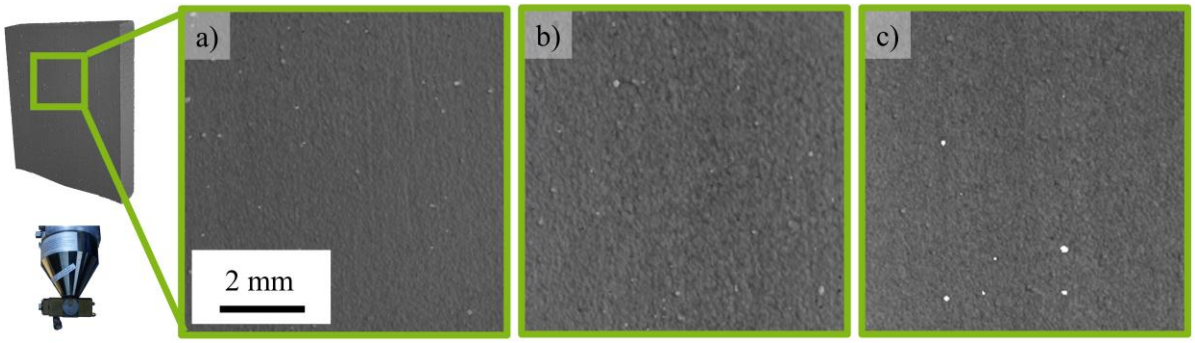

Figure 8: Surface condition of Al within a bonded CFRP/Al hybrid with digitally removed CFRP layer for a) non-structured and b), c) laser-structured material, b) parameter set 1, c) parameter set 2.

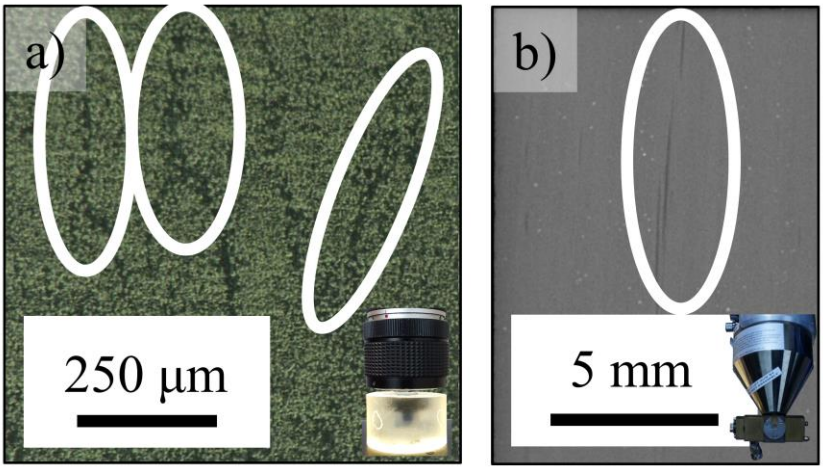

Figure 9:Irregular shift of carbon fibers a) in longitudinal direction (top view) via LM and b) in fiber direction (front view) via CT

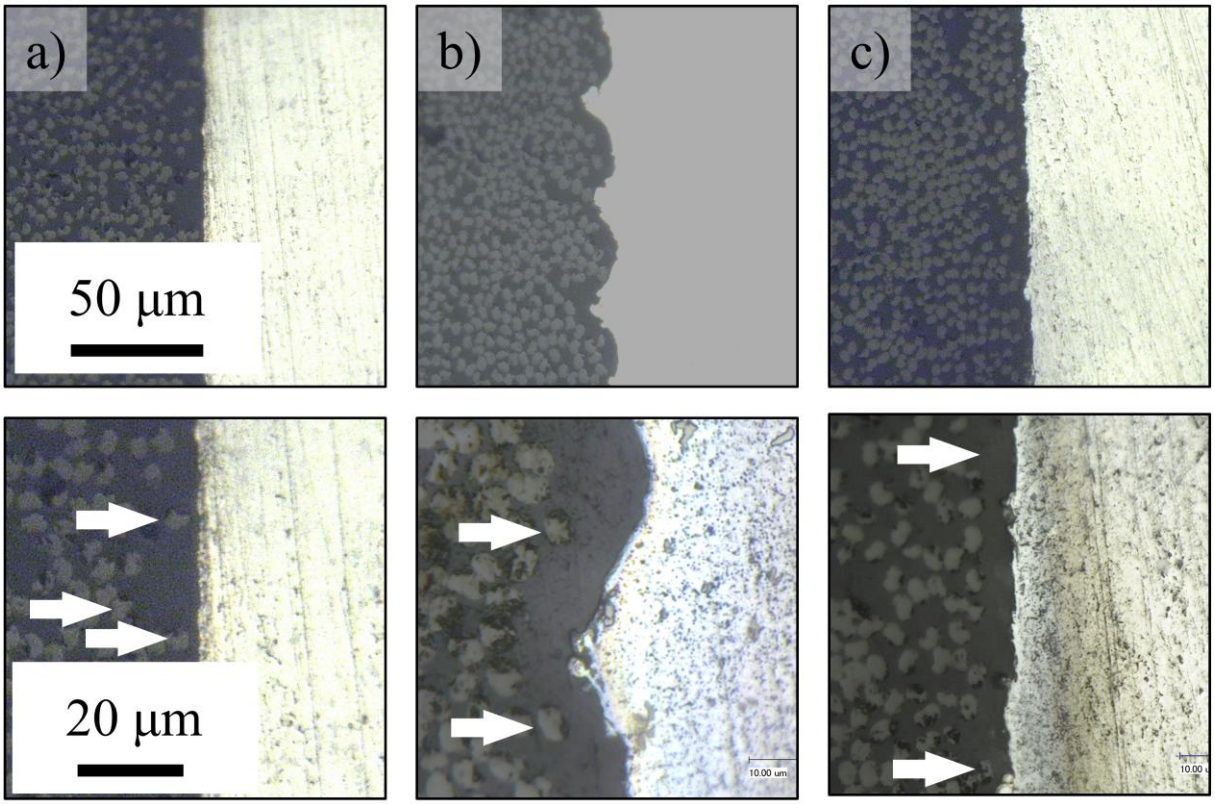

Figure 10: Close-up of the CFRP (left side)/Al (right side) interface with different surface structuring of Al (top) and detailed view on the fiber-Al distances (bottom), for a) a non-structured surface, b) parameter set 1 and c) parameter set 2.

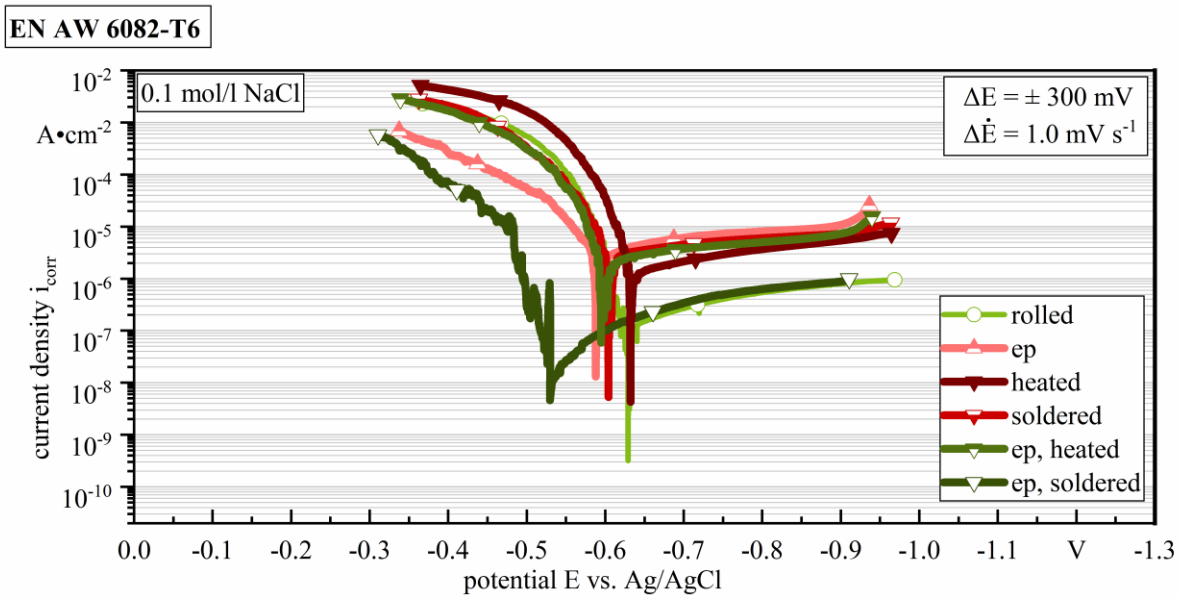

Figure 11: Condition of CFRP (top)/Al (bottom) hybrid material before and after corrosion as viewed from the specimens' top: Without structuring: a) initial, b) corroded; Parameter 1: c) initial, d) corroded; Parameter 2: e) initial, f) corroded.

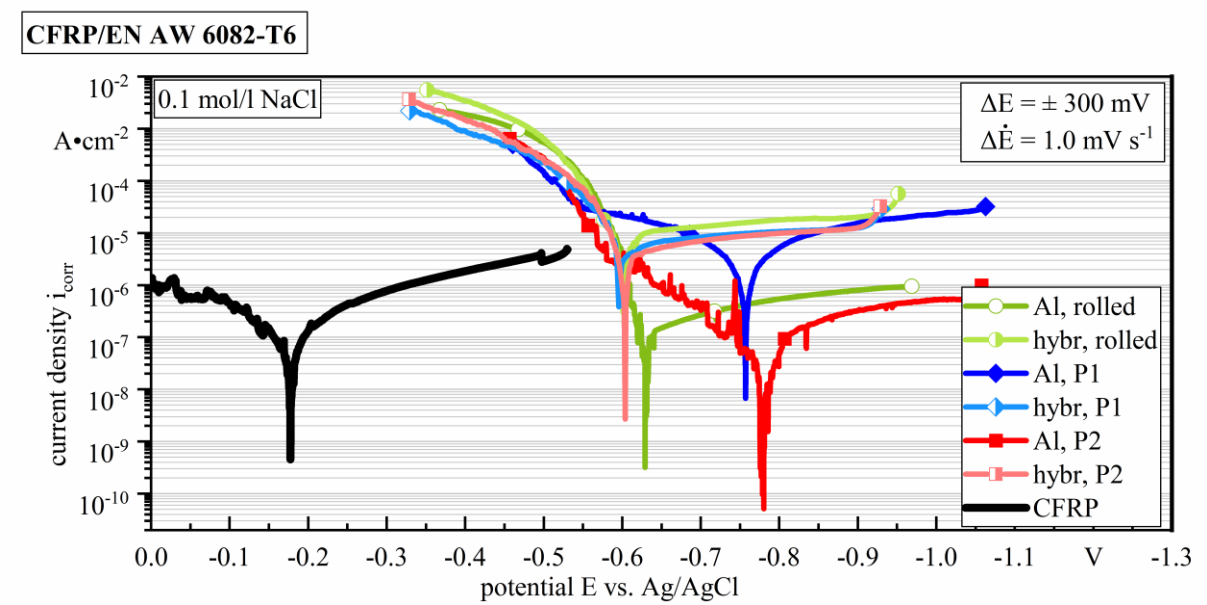

Figure 12: Tafel plot of EN AW 6082-T6 with varying surface and contacting condition: initial condition without treatment, electrolytically polished (ep), soldered and heated.

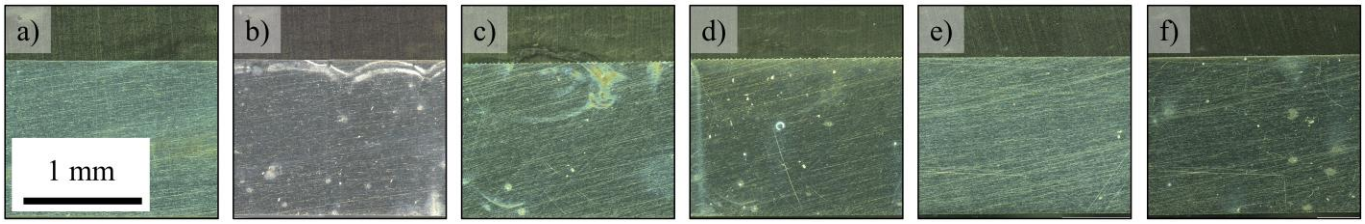

Figure 13: Micrographs of pre- and post-corrosion surfaces a), b) non-structured (Al, rolled), c), d) structured (Al, P1), e), f) structured (Al, P2)

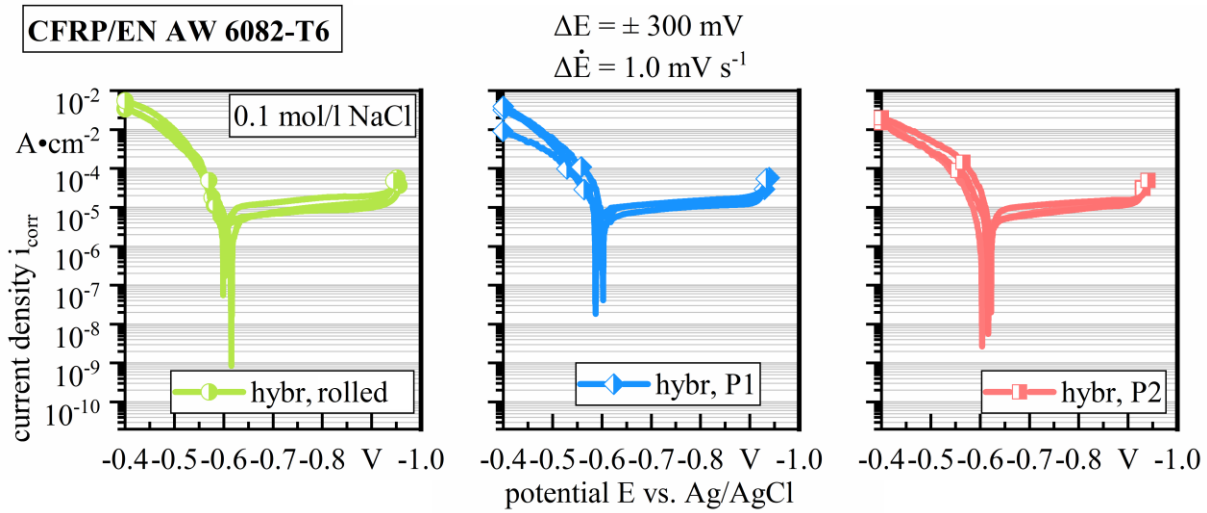

Figure 14:Tafel plot of three PDP-measurements for pristine, P1 and P2 hybrids